Examining the Impacts of Great Lakes Temperature Perturbations on Simulated Precipitation in the Northeastern United States

JANEL HANRAHAN,[a] JESSICA LANGLOIS,[a] LAUREN CORNELL,[b] HUANPING HUANG,[c] JONATHAN M. WINTER,[d] PATRICK J. CLEMINS,[e,f] BRIAN BECKAGE,[f,g] AND CINDY BRUYÈRE[h]

[a] *Department of Atmospheric Sciences, Northern Vermont University–Lyndon, Lyndonville, Vermont*
[b] *State University of New York College of Environmental Science and Forestry, Syracuse, New York*
[c] *Climate and Ecosystem Sciences Division, Lawrence Berkeley National Laboratory, Berkeley, California*
[d] *Department of Geography, Dartmouth College, Hanover, New Hampshire*
[e] *Vermont EPSCoR Program, University of Vermont, Burlington, Vermont*
[f] *Department of Computer Science, University of Vermont, Burlington, Vermont*
[g] *Department of Plant Biology, University of Vermont, Burlington, Vermont*
[h] *National Center for Atmospheric Research, Boulder, Colorado*

(Manuscript received 29 July 2020, in final form 1 June 2021)

ABSTRACT: Most inland water bodies are not resolved by general circulation models, requiring that lake surface temperatures be estimated. Given the large spatial and temporal variability of the surface temperatures of the North American Great Lakes, such estimations can introduce errors when used as lower boundary conditions for dynamical downscaling. Lake surface temperatures (LSTs) influence moisture and heat fluxes, thus impacting precipitation within the immediate region and potentially in regions downwind of the lakes. For this study, the Advanced Research version of the Weather Research and Forecasting Model (WRF-ARW) was used to simulate precipitation over the six New England states during a 5-yr historical period. The model simulation was repeated with perturbed LSTs, ranging from 10°C below to 10°C above baseline values obtained from reanalysis data, to determine whether the inclusion of erroneous LST values has an impact on simulated precipitation and synoptic-scale features. Results show that simulated precipitation in New England is statistically correlated with LST perturbations, but this region falls on a wet–dry line of a larger bimodal distribution. Wetter conditions occur to the north and drier conditions occur to the south with increasing LSTs, particularly during the warm season. The precipitation differences coincide with large-scale anomalous temperature, pressure, and moisture patterns. Care must therefore be taken to ensure reasonably accurate Great Lakes surface temperatures when simulating precipitation, especially in southeastern Canada, Maine, and the mid-Atlantic region.

KEYWORDS: Inland seas/lakes; Precipitation; Water budget/balance; Climate models; Model evaluation/performance; Regional models

1. Introduction

Data from general circulation models (GCMs) are often not resolved at a scale that provides information about inland water bodies. When downscaling GCM output with a regional climate model (RCM) over a domain that includes large lakes, lower boundary conditions for such features may therefore not exist within the driving dataset. However, because lakes can have a strong influence on regional air temperature and precipitation (Scott and Huff 1996; Anyah and Semazzi 2004; Notaro et al. 2013; Wright et al. 2013), this information may be critical when simulating weather and climate.

When water surfaces such as oceans and lakes are resolved within the driving dataset, regional climate models, including the Weather Research and Forecasting (WRF) Model, apply their temperatures to the corresponding water points in the new simulation domain. When water surface data are not provided by the driving dataset, the default treatment in WRF is to substitute values from the nearest grid cells for which water surface temperatures are available. This method is likely suitable for water bodies that are partially resolved, ensuring that values are borrowed from neighboring, or at least nearby, grid cells. However, water bodies that are completely unresolved and also geographically isolated, such as inland lakes, could assume unrealistic properties from a remote location (Wang et al. 2017). For the North American Great Lakes, which are often completely unresolved by GCMs, the nearest grid cells are usually located in the Atlantic Ocean and Hudson Bay. This method can introduce unrealistic temperature discontinuities, sometimes as large as 20°–30°C from one model grid cell to the next, and substantial temperature biases (Gao et al. 2012; Mallard et al. 2015). Spero et al. (2016) investigated how incongruous Great Lakes temperatures influence regional climate extremes by comparing WRF simulations when this nearest-neighbor approach was used with simulations that employed a lake model instead. The differences in lake surface temperatures (LSTs) between these two approaches were large. Those assigned by WRF during preprocessing were 14° and 23°C warmer during July and December, respectively, than those assigned by the lake model. They determined that

Supplemental information related to this paper is available at the Journals Online website: https://doi.org/10.1175/JAMC-D-20-0169.1.

Corresponding author: Janel Hanrahan, janel.hanrahan@northernvermont.edu

DOI: 10.1175/JAMC-D-20-0169.1

the erroneous temperatures introduced with the former setting produced large-scale artifacts such as thermally induced waves. The impacts on simulated precipitation and temperature were thus not limited to the immediate Great Lakes region, but instead extended across much of the eastern half of the United States.

An alternative method provided in the WRF Preprocessing System (WPS) allows the user to assign temporally averaged 2-m air temperatures from collocated land points to the underlying lake surfaces [see Wang et al. (2017) and Mallard et al. (2015) for detailed descriptions of this method]. When employing this alternative LST method, the user must define the interval over which temperatures are averaged, and if desired, a time lag may be introduced to account for differences in thermal inertia. Bullock et al. (2014) concluded that this method did not produce realistic temperatures or ice cover, and that when available, higher-resolution GCM or reanalysis data should instead be used. Because both these methods assign lower boundary conditions for LSTs that do not allow for physically realistic responses to regional and spatial atmospheric changes, the lakes do not come into equilibrium with the overlying atmosphere throughout the model simulation (Spero et al. 2016).

For historical simulations, observed lake temperature data may be assimilated, but LST values can vary greatly from one data source to the next. For example, Zhao et al. (2012) identified differences between satellite-derived and reanalysis wintertime Great Lakes surface temperatures in excess of 8°C. For model simulations completed during future time periods, LST observations do not exist, so the simplest approach may be to assume steady-state values obtained from higher-resolution climatological data (Mallard et al. 2015). Great Lakes surface temperatures, however, are highly variable in space and time, as is ice cover extent during the cold season (Wang et al. 2012). Interannual surface temperature changes for individual lakes can approach 10°C (Zhong et al. 2016), the seasonal cycle typically produces a LST range of 20°C, and daily lake-to-lake temperature differences average more than 5°C (see Tables S1 and S2 in the online supplemental material).

Another complicating factor for estimating LSTs is the increase in surface temperatures of the North American Great Lakes over the past few decades (Zhong et al. 2016). This is consistent with the warming of lakes worldwide under anthropogenic global warming, particularly at mid- to high latitudes (Schneider and Hook 2010; O'Reilly et al. 2015). The observed rate of water temperature increase is generally larger than that of the surrounding air, resulting in increasing evaporative losses (Hunter et al. 2015), and modified precipitation in nearby regions (Hayhoe et al. 2010; Gula and Peltier 2012; Zhao et al. 2012; Wright et al. 2013). Great Lakes surface temperatures are likely to continue increasing into the future, particularly during the warm season. Because this accelerated warming may be driven by decreasing wintertime ice cover, such trends will continue at least for another few decades until the lakes become ice-free year-round, at which time the lakes are expected to warm at a rate more consistent with the regional atmosphere (Austin and Colman 2007). Observed real-world impacts of disproportionate LST trends underscore the need to ensure their accuracy when simulating regional weather and climatology.

Coincident with the timing of recent elevated evaporative losses from the Great Lakes (Hanrahan et al. 2010; Hunter et al. 2015), annual precipitation and associated cloud cover have been increasing in the northeastern United States in recent decades (Guilbert et al. 2015; Hoerling et al. 2016; Huang et al. 2017), particularly during the warm season (Easterling et al. 2017; Hanrahan et al. 2017). While the closest New England state is more than 200 km from the Great Lakes, the surface area of the lakes is approximately 30% larger than the combined land area of New England. Given that annual evaporative losses from some of the lakes can approach depths of 100 cm (Hunter et al. 2015), which is comparable to annual precipitation totals in the northeastern United States (Huang et al. 2017), changes in LST values and subsequent evaporative losses have the potential to substantially modify precipitation in this downwind region, purely from a water balance perspective. Therefore, as modeling studies seek to understand the underlying causes for precipitation trends, and to provide accurate long-term forecasts in New England under anthropogenic climate change, it is important to examine whether LST accuracy is a critical factor when simulating weather in this region.

For this work, we use an approach of systematically increasing and decreasing Great Lakes temperatures to examine how this may influence simulated precipitation downwind of the lakes during a recent 5-yr period. Our study region is New England, which includes the states of Maine, Vermont, New Hampshire, Massachusetts, Connecticut, and Rhode Island (Fig. 1, outlined in blue). In section 2, we describe the RCM configuration, identify the driving datasets, and discuss how the LSTs were modified. We then examine precipitation dependence within New England, and atmospheric dynamics over the larger northeastern U.S. region, on these LST changes in section 3, and the results are discussed in section 4.

2. Methods and data

The Advanced Research version of the Weather Research and Forecasting Model (WRF-ARW), version 3.9.1 (Skamarock et al. 2019), was used to simulate precipitation over the northeastern United States during 2010–14. Two one-way nests were used with an outer-domain (D1) resolution of 36 km and an inner-domain (D2) resolution of 12 km (Fig. 1). The domain configuration used here is similar to those used in other modeling studies that examine climate in the New England region, with respect to location and resolution (e.g., Gao et al. 2012; Trail et al. 2013; Burakowski et al. 2016; Komurcu et al. 2018).

Initial and lateral boundary conditions were obtained from European Centre for Medium-Range Weather Forecasts (ECMWF) ERA-Interim, which has an approximate spatial resolution of 80 km (Dee et al. 2011). Physics options for both domains are identified in Table 1. Radiation, cumulus, microphysics, and boundary layer schemes were selected on the basis of optimal model performance in this region as discussed in Huang et al. (2020).

Information about some of the Great Lakes is included in the ERA-Interim dataset, but there are substantial regions

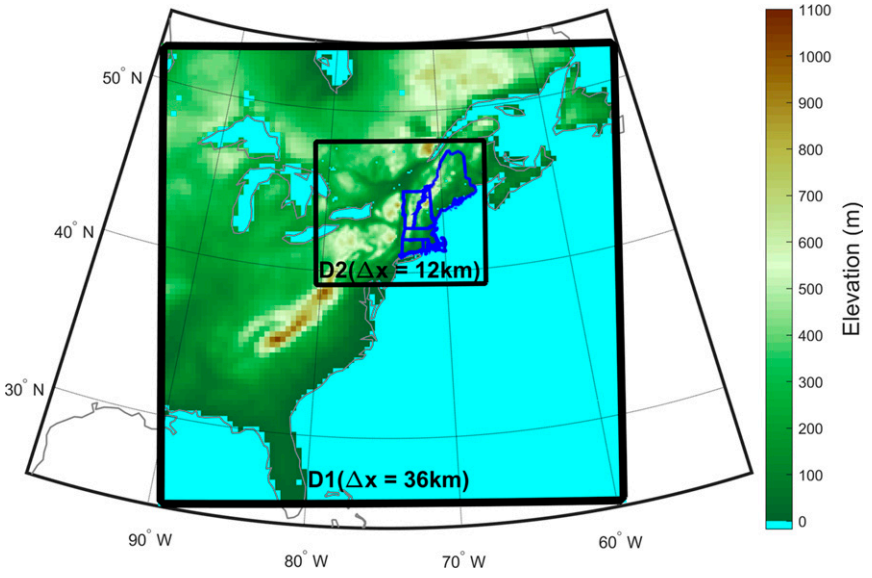

FIG. 1. WRF Model domains (black outlines) and region of interest (blue outlines).

where LST data do not exist (Fig. 2). We thus replaced existing values, and filled in missing LSTs, with daily averaged lake temperatures from ECMWF's latest global reanalysis, ERA5 (Copernicus Climate Change Service 2017) using the nearest-neighbor approach. This was done prior to the WRF simulation by modifying WPS met_em files, which contain preprocessed horizontally interpolated meteorological data as required for WRF simulations. Because ERA5 data are available at a resolution of 30 km, which is comparable to our D1 resolution of 36 km, this produced a more complete picture of the Great Lakes temperatures (Fig. 2). In addition to replacing LST values, all ice information was removed, resulting in zero ice cover for all of the lakes. Instead of interpolating lake ice cover from the driving dataset, a freezing temperature threshold was set at −1°C (272 K) in WRF. A surface grid cell situated over the lakes is therefore treated as ice when the water temperature drops just below freezing. We opted for an ice threshold slightly below the freshwater freezing point to avoid erroneous freezing of ocean waters, which have a lower freezing temperature threshold.

Once the LSTs were replaced with the baseline ERA5 data for each day during 2010–14, 10 additional directories were created that contained identical WPS files. LSTs were then perturbed by increasing or decreasing values uniformly across all Great Lakes grid cells (Figs. 3 and 4). The temperature perturbations were $\Delta T = \pm 1°, 2°, 4°, 8°$, and 10°C, with a lower bound temperature of $T = -2$°C. While observed LSTs do not fall below 0°C, this lower bound was selected to allow ice formation on the lakes, which was set to occur when temperatures drop below the −1°C threshold. Note that the imposition of a lower bound lessens the extent to which some LSTs are actually reduced when the baseline temperature is already relatively cold, thus resulting in identical LSTs for some of the negative-perturbation simulations during the cold months. The span of 20°C was chosen to encompass spatial and temporal LST variability (Zhong et al. 2016), the magnitude of errors that may be introduced through various methods of LST approximation (Zhao et al. 2012; Mallard et al. 2015), and the observed range of temperature increases over the past few decades (Hanrahan et al. 2010; Schneider and Hook 2010; Hunter et al. 2015; O'Reilly et al. 2015; Zhong et al. 2016; Easterling et al. 2017).

All five simulation years were completed simultaneously and initialized on 1 December of the previous year, allowing for a 1-month spinup period. Analyses included here consider only data from 1 January to 31 December of the simulation year. For our seasonal analysis, winter is defined as January, February, and December of the same calendar year, and for the remaining seasons, the usual meteorological definitions are used (spring = March–May, summer = June–August, and fall = September–November). While winter as it is defined here deviates from the usual December–February convention, the subsequent analysis considers only seasonal statistics. Thus, the replacement of simulated data for December 2009 with December 2014, only 1 of the 15 total months for winter, is an acceptable substitution in lieu of eliminating data for the 2010 winter altogether.

A total of 55 simulations were completed, consisting of 11 LST perturbations ($\Delta T = 0$ and $\pm 1°, 2°, 4°, 8°$, and 10°C) for

TABLE 1. WRF configuration for both model domains.

Microphysics	WSM6 (Hong and Lim 2006)
Radiation physics (long- and shortwave)	RRTMG (Iacono et al. 2008)
Surface layer physics	Revised MM5 Monin–Obukhov (Jiménez et al. 2012)
Land surface physics	Thermal diffusion scheme
Boundary layer physics	YSU scheme (Hong and Lim 2006)
Cumulus parameterization	New simplified Arakawa–Schubert scheme

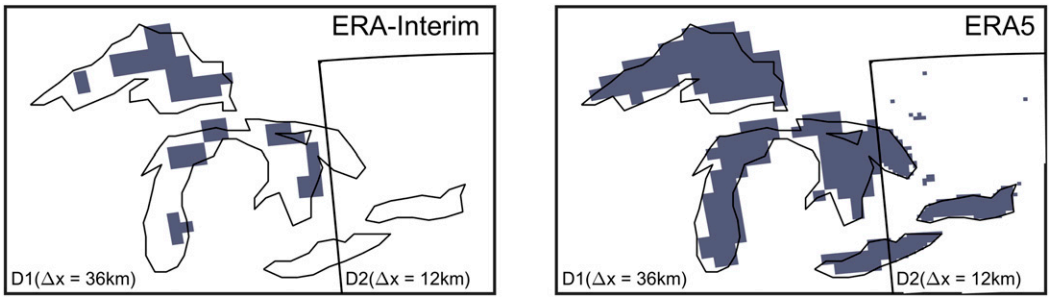

FIG. 2. Lake temperature data (shaded regions) available within WRF domains. The (left) raw temperature field provided by the ERA-Interim reanalysis is replaced by (right) the higher-resolution ERA5 reanalysis.

each of the five years, hereinafter referred to as LST^{-10}, LST^{-8}, LST^{-4}, LST^{-2}, LST^{-1}, LST^{0}, LST^{+1}, LST^{+2}, LST^{+4}, LST^{+8}, and LST^{+10}. We applied a threshold to the simulated precipitation data of 1 mm. Grid cells where daily precipitation met or exceeded 1 mm were thus defined as wet days, while grid cells with precipitation of less than 1 mm were defined as dry days and the values were replaced with zero (Frich et al. 2002).

3. Results

a. Simulated evaporation and ice cover

Simulated annual area-averaged evaporative losses from the Great Lakes average 2.7 mm day^{-1} for the baseline simulation, LST^{0}, ranging from 0.7 mm day^{-1} during spring to 4.2 mm day^{-1} during fall (Fig. 5a). These values are similar in magnitude to recent overlake evaporation estimates in the NOAA/Great Lakes Environmental Research Laboratory monthly hydrometeorological database (Fig. 10 in Hunter et al. 2015) of approximately 0.8 mm day^{-1} during the month of April and 4.0 mm day^{-1} during October–December. Simulated evaporative losses approach 18 mm day^{-1} during summer and fall for LST^{+10} and decrease to nearly zero for all seasons in LST^{-10}.

Simulated area-averaged ice cover for the lakes is zero during summer and fall, 7.5% during winter, and 11% during spring, for the baseline simulation (Fig. 5b). These values are less than the observed 2010–14 average of 16.6% in winter and 12.7% in spring but are within the observed range during this period of 3.8%–40.2% and 1.1%–43.9% (see Table S3 in the online supplemental material). We note that an increase of ice cover from winter to spring is atypical based on the observed data and we speculate that this discrepancy results from the overly simplified relationship of ice formation whenever the water temperature drops below −1°C in WRF. As illustrated in Fig. 4, simulated LSTs decreased until January–February and remained at the lowest annual temperatures throughout the spring months coincident with the timing of the highest simulated ice cover. Despite this result, an increase in ice cover from winter to spring does occur in the real world (as

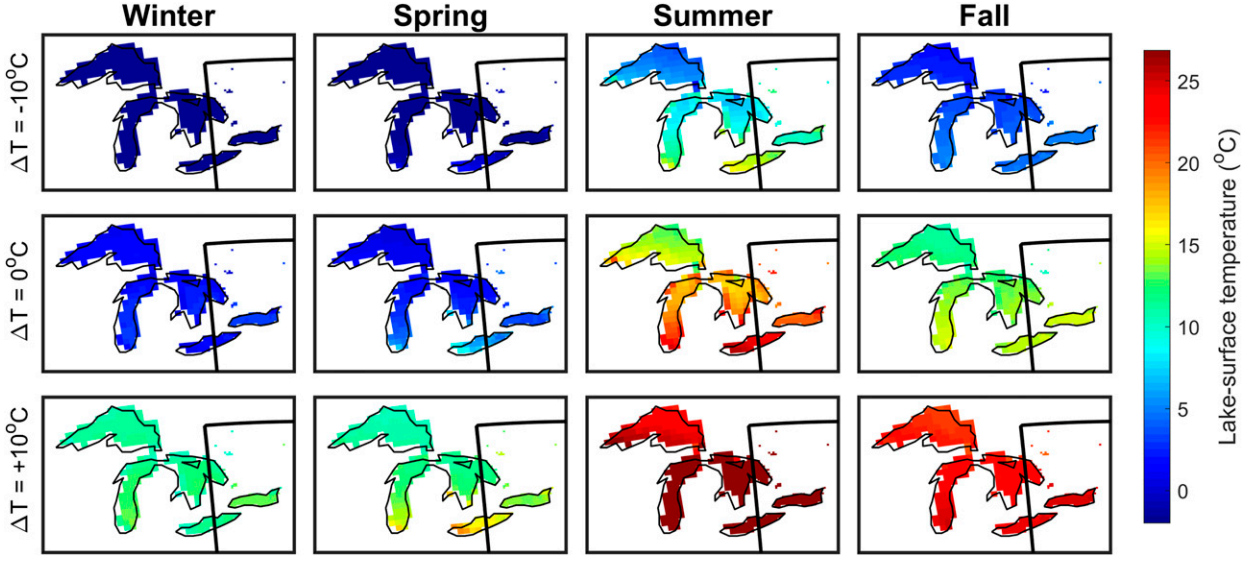

FIG. 3. Averaged seasonal lake-surface temperatures during 2010–14 as provided by ERA5 with (top) $\Delta T = -10$°C, (middle) $\Delta T = 0$°C, and (bottom) $\Delta T = +10$°C.

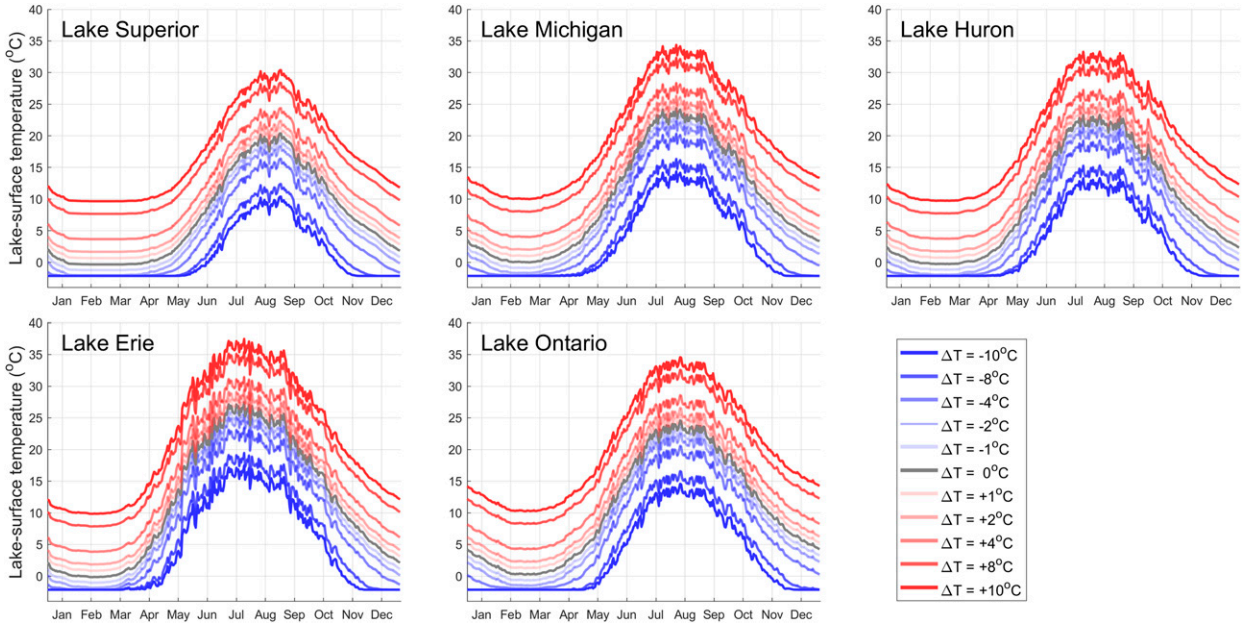

FIG. 4. Spatially and temporally averaged daily lake-surface temperatures during 2010–14 as provided by ERA5 (gray lines) and $\Delta T = \pm 1°, 2°, 4°, 8°$, and 10°C (blue and red lines). Averages are computed over D1 for lakes outside D2 and over D2 for lakes included in this region.

was the case in 2014), and the magnitude of cold-season values overall are reasonable. For LST^{-10}, simulated wintertime ice cover is 100%, and approximately 10% of the lakes remain frozen during the warm season, with Lake Superior remaining at least partly frozen year-round and Lake Ontario completely ice free for four months of the year (see Table S4 in the online supplemental material). By LST^{-4} the lakes are virtually ice free during summer and fall and about 68% ice covered during winter and spring, and by LST^{+1}, the lakes remain ice free year-round.

We conclude that evaporative losses and ice cover extent as simulated by WRF are sensitive to lake temperatures. This dependence is expected, with increasing (decreasing) evaporative losses and decreasing (increasing) ice cover with warmer (cooler) lake water. Furthermore, we find that the simulated evaporation and ice cover values obtained from the baseline simulations, LST^0, are comparable to observation.

b. *Simulated precipitation in New England*

1) SPATIALLY AVERAGED PRECIPITATION

Spatially averaged annual and seasonal simulated precipitation within the New England region (Fig. 1, outlined in blue) is plotted in Fig. 6 for all simulation years, against LST perturbations $\Delta T = \pm 1°, 2,° 4°, 8°$, and 10°C, with lines of best fit. A limitation of this presentation is that the most negative perturbations during some months of winter and spring are not

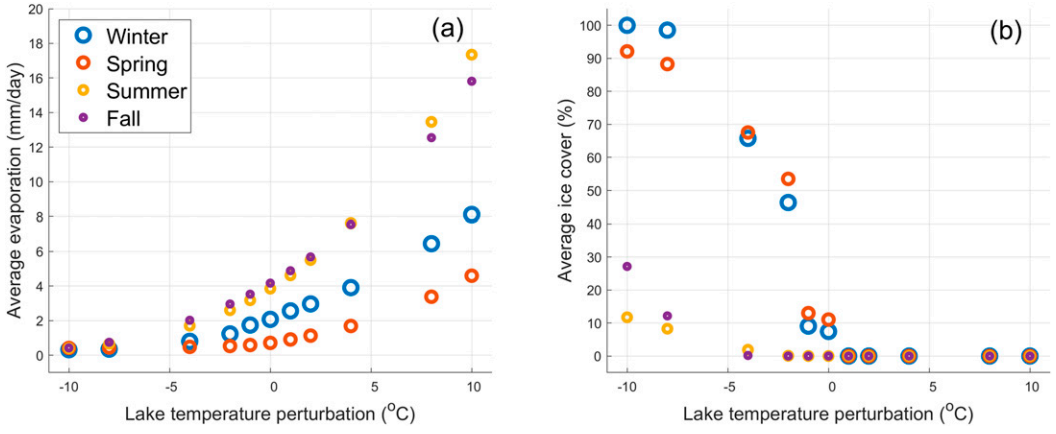

FIG. 5. Average simulated (a) evaporative losses (mm day^{-1}) and (b) ice cover (%) per season for the Great Lakes.

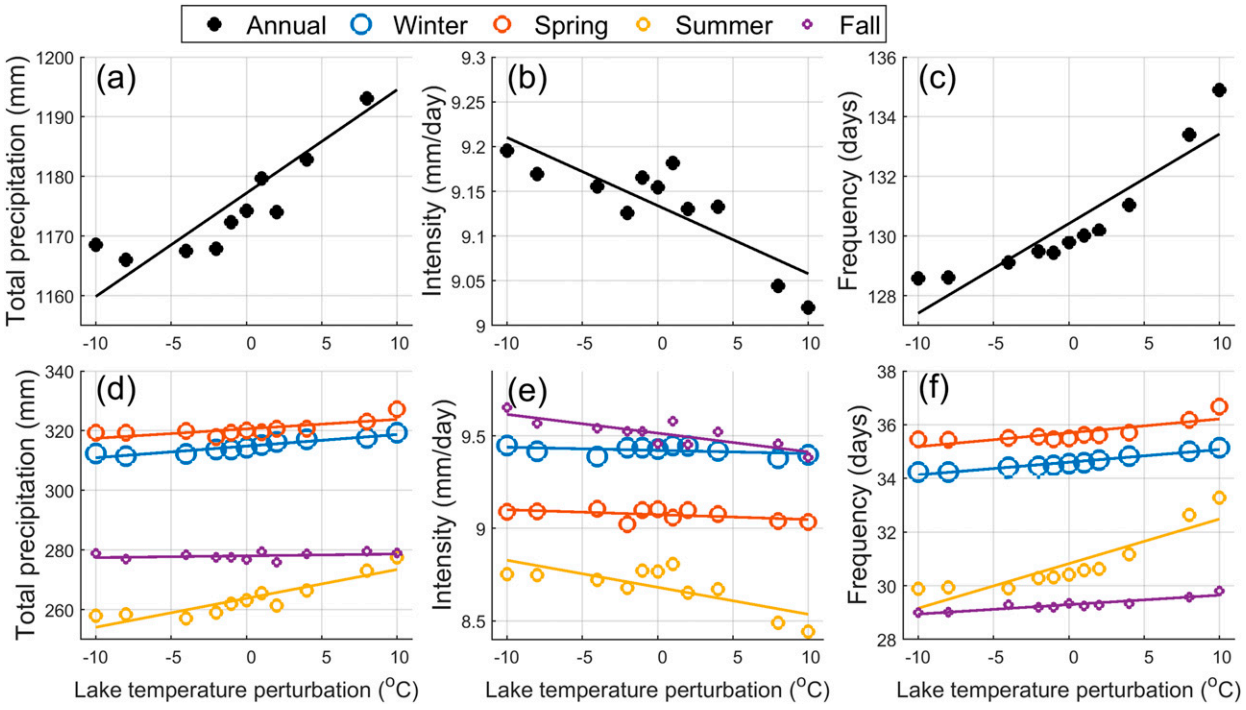

FIG. 6. Spatially and temporally averaged simulated (a)–(c) annual and (d)–(f) seasonal precipitation (left) totals, (center) intensity, and (right) frequency, with lines of best fit, within the New England region.

fully realized given the imposition of a lower bound in LST values. For actual LSTs coinciding with each ΔT identified here, the reader is referred to Fig. 4. Precipitation is quantified as total depth (mm) in Figs. 6a and 6d, average intensity (mm day^{-1}, including only wet days) in Figs. 6b and 6e, and frequency (number of wet days) in Figs. 6c and 6f. Regression analysis results are shown in Table 2, which includes r^2, results of significance testing at the 5% level (indicated in boldface font), and slope values (precipitation metric/LST perturbation).

We find a statistically significant correlation ($p < 0.05$), with $r^2 = 0.81$, between spatially and temporally averaged annual total precipitation and Great Lakes temperature perturbation, with a slope of +1.73 mm of annual precipitation per degree Celsius change in LST (Fig. 6a and Table 2). The LST^{-10} to LST^{+10} difference of about 30 mm is 3% of the annual simulated total for the New England region during this 5-yr period.

When considering individual seasons, we find that more than one-half of the dependent total precipitation on LST occurs during the summer with a slope of +0.97 mm °C^{-1}. The summertime LST^{-10} to LST^{+10} difference of 20 mm makes up about 7% the seasonal total precipitation. Most of the remaining dependent total precipitation occurs during winter and spring, with slopes of +0.39 and +0.32 mm °C^{-1}, respectively. Given the combination of relatively small slope values, and high total precipitation amounts, the LST^{-10} to LST^{+10} differences only make up about 2% of the seasons' total precipitation. We further conclude that there is no statistical correlation between LST perturbation and total precipitation during the fall season.

Regionwide annual average precipitation intensity slightly decreases with increasing LSTs, particularly during the summer and fall seasons. While the dependence is statistically significant during these seasons, the LST^{-10} to LST^{+10} decrease in intensity is only 2%–3% of the seasonal averages,

TABLE 2. Results of regression analysis comparing total area-averaged simulated precipitation in New England with Great Lake temperature perturbations. Boldface values indicate statistically significant correlations ($p < 0.05$).

	Total precipitation (mm)		Daily intensity (mm day^{-1})		Frequency (days)	
	Slope (mm °C^{-1})	r^2	Slope (mm °C^{-1})	r^2	Slope (days °C^{-1})	r^2
Annual	**+1.73**	**0.81**	**−0.008**	**0.71**	**+0.30**	**0.83**
Winter	**+0.39**	**0.90**	−0.002	0.19	**+0.05**	**0.96**
Spring	**+0.32**	**0.58**	−0.003	0.27	**+0.05**	**0.66**
Summer	**+0.97**	**0.82**	**−0.015**	**0.57**	**+0.17**	**0.80**
Fall	+0.06	0.09	**−0.010**	**0.69**	**+0.04**	**0.85**

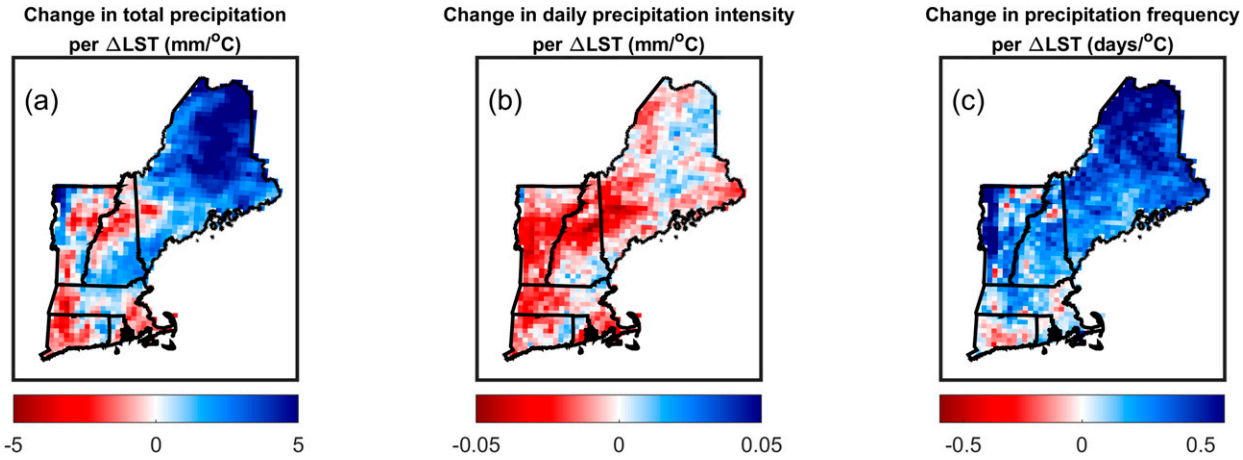

FIG. 7. Slopes of best-fit regression lines for each modeled grid cell within New England, quantified as change in simulated annual precipitation (a) totals (mm), (b) intensity (mm), and (c) frequency (days) per LST perturbation (°C). Blue shading indicates wetter conditions, and red shading indicates drier conditions, with increasing LSTs.

thus only minimally contributing to the seasonal and annual changes in precipitation totals. Precipitation frequency increases during all seasons with increasing LSTs, with the largest increase during the summer season of about three days, or about 10% of the seasonal average.

We conclude that changes in Great Lakes surface temperatures modify area-averaged simulated total precipitation in New England, but only by a small amount relative to the annual total. More than one-half of the dependent total precipitation, however, occurs during the summer. The increase in annual precipitation totals with warmer LSTs is the result of an increase in the number of wet days each year, half of which occur during the summer, but is slightly moderated by decreasing precipitation intensity on these days.

2) SPATIAL VARIABILITY OF PRECIPITATION

To better understand the dependence of precipitation in New England on LST perturbations (or lack thereof), we next examined the spatial structure by plotting slope values of the best-fit regression lines for each grid cell within the New England region (Fig. 7). Slopes are defined as precipitation metric divided by LST perturbation, where the metrics are total precipitation (Fig. 7a), average intensity (Fig. 7b), and frequency (Fig. 7c).

The dependence of total annual precipitation on LST is heterogeneous across the region, with the largest positive slope of about 5 mm $°C^{-1}$ occurring across much of Maine (Fig. 7a, blue regions), and the most negative slope of about 3 mm $°C^{-1}$ in isolated regions across the remaining states (Fig. 7a, red regions). A reduction of average precipitation intensity with increasing LSTs is evident across much of the region with the largest decreases of about 0.05 mm day^{-1} $°C^{-1}$ occurring throughout Vermont, northern New Hampshire, and western Massachusetts (Fig. 7b, red regions), and slight intensity increases across eastern Maine, southern New Hampshire, and eastern Connecticut (Fig. 7b, blue regions). There is an increasing number of wet days with increasing LSTs across most of New England (Fig. 7c, blue regions), with the exception of a slight decrease throughout Connecticut and a few isolated spots in other states (Fig. 7c, red regions).

This examination of spatial variability reveals that the precipitation dependence on perturbed Great Lakes surface temperatures is not uniform across New England. Some states are disproportionately impacted by changing LSTs, particularly Maine, with precipitation metric values that are notably larger than the areawide averages identified in Fig. 6 and Table 2.

c. *Simulated precipitation beyond New England*

To obtain a sense of the synoptic-scale spatial patterns associated with incremental changes in LSTs, we examined simulated precipitation across the entire inner domain (D2), and adjacent regions of the outer domain (D1), for each metric. For this analysis, total precipitation (Fig. 8), average precipitation intensity (Fig. 9), and precipitation frequency (Fig. 10), are quantified as differences in metrics between $\Delta T = \pm 1°$, 4°, and 10°C simulations and the baseline simulation ($\Delta T = 0°C$). For example, the $\Delta T = \pm 10°C$ row includes the precipitation from the LST^{+10} simulation minus precipitation from the LST^{0} simulation as illustrated in the top row. Only means that are significantly different from the baseline values according to a two-sided t test ($p < 0.05$) are shown, with increased values in blue and decreased values in red.

We find that the general pattern of wetter conditions to the north and drier conditions to the south for LST^{+}, extends well beyond the New England region. Seasonal precipitation totals (Fig. 8) have a large-scale bimodal distribution that is amplified with increasing magnitude of LST perturbations. In general, as LSTs increase, total precipitation increases directly over the Great Lakes, as well as to the north and northeast of this region. At the same time, total precipitation generally decreases to the south and southeast. The present area of interest is located at the intersection of these precipitation modes. Maine is situated in the wetter region, while the other New England

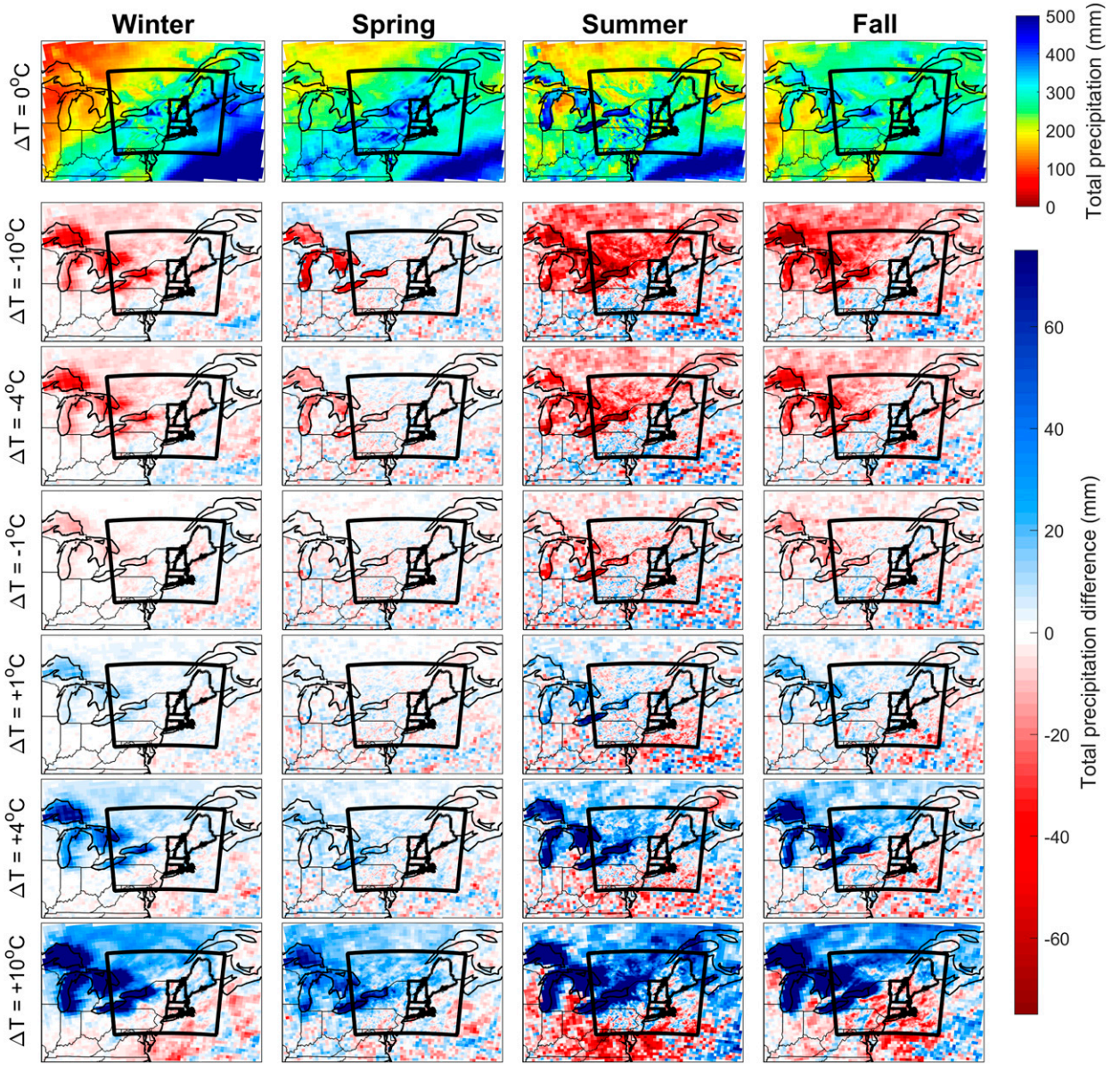

FIG. 8. (top) Total simulated seasonal precipitation, and difference in seasonal average total precipitation between $\Delta T = \pm 1°$, 4°, and 10°C simulations and the $\Delta T = 0$°C simulation. Only means that were significantly different from the baseline simulation according to a two-sided t test ($p < 0.05$) are shown.

states are generally within the drier region for LST^{+}. This bimodal spatial pattern generally exists during all seasons, with the strongest signal emerging during summer and fall. While this wet–dry pattern is most prominent for LST^{-10} and LST^{+10}, distinct wet and dry regions begin to emerge well outside the Great Lakes region, including much of southeastern Canada, by LST^{-4} and LST^{+4}. With LST perturbations of LST^{-10} and LST^{+10}, simulated precipitation differences are in excess of 40 mm in some areas as far as 1000 km from the Great Lakes.

To examine how these differences arise, average precipitation intensity is illustrated in Fig. 9 (mm day^{-1}) and frequency is shown in Fig. 10 (number of wet days). The bimodal pattern is visible in both precipitation metrics but is more strongly represented by precipitation frequency. For LST^{+10}, more frequent wet days occurred directly over and to the northeast of the lakes, while fewer wet days occurred in these regions for LST^{-10} during winter, summer, and spring. The frequency metric spatial patterns (Fig. 10) thus largely mirror those for the total precipitation (Fig. 8) with a few exceptions. During spring, there were more frequent wet days over the lakes and much of the surrounding area for LST^{+10}, but average intensity had decreased over most of the lakes, thus lessening the increase in total seasonal precipitation. In addition, during summer, LST^{+10} had slightly fewer wet days directly to the

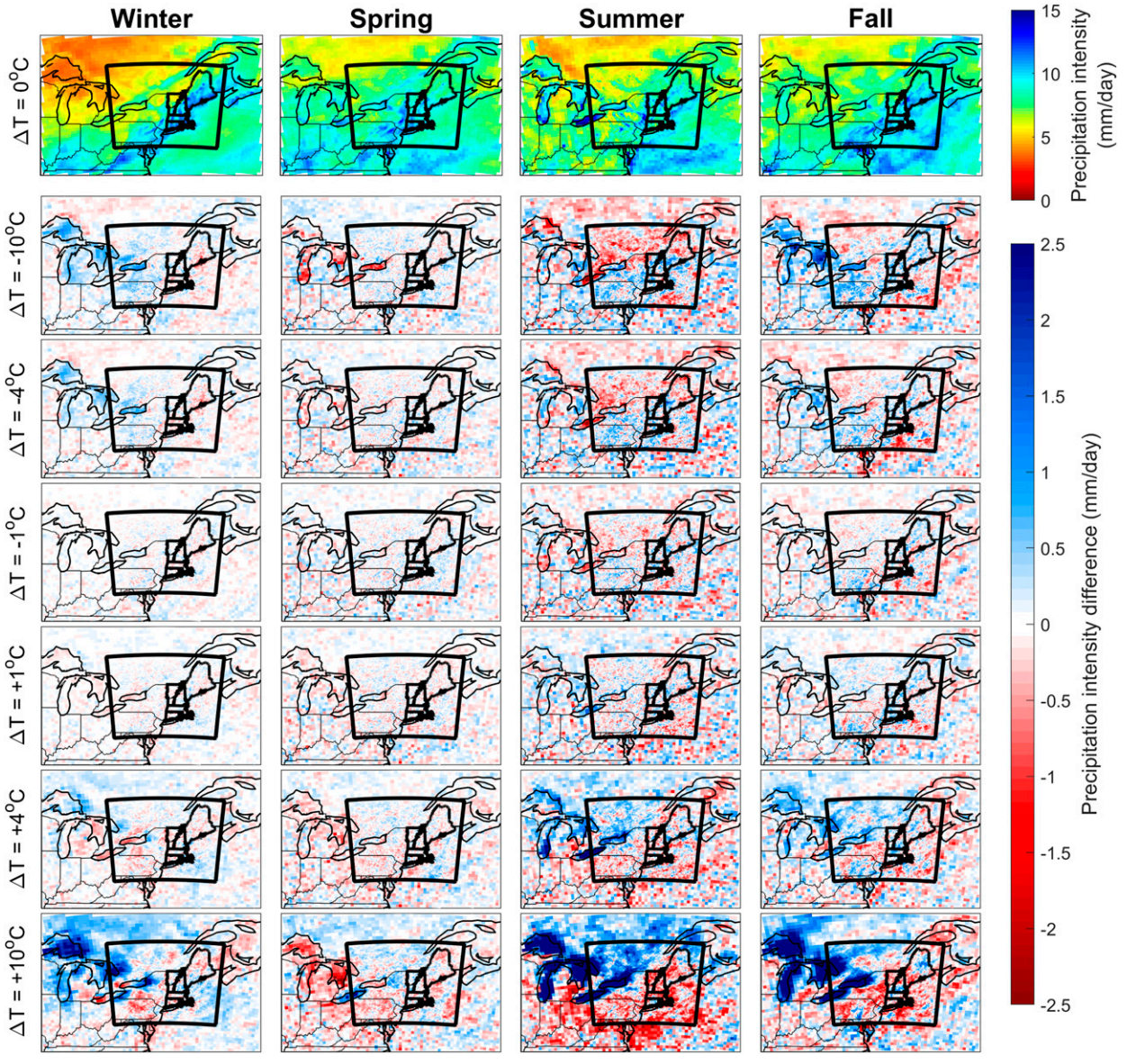

FIG. 9. As in Fig. 8, but for precipitation intensity (average precipitation per wet day).

north of the upper lakes that was opposed by more intense precipitation, thus resulting in more total precipitation in this region.

We note that there are some discontinuities between model domains, resulting in a few instances of abrupt differences in precipitation metrics from the outer edge of the inner domain (D2) and the neighboring grid cells in the outer domain (D1). However, we conclude that these model artifacts are well outside the northeastern region and should not hinder the analyses presented here.

d. Synoptic-scale differences in other atmospheric variables

To understand dynamical drivers behind the differences in precipitation with increasing and decreasing LSTs, we examined differences between atmospheric variables for LST^{-10} and LST^{+10}, by again subtracting out the baseline LST^{0} values. As illustrated in Fig. 11, 2-m temperatures largely mirror the lake-temperature perturbations, with warmer air temperatures directly over the lakes when LSTs are warm and colder air temperatures when LSTs are cold. Statistically significant ($p < 0.05$) 2-m temperature differences extend to locations far from the lakes, particularly for LST^{+10} during fall and winter. This warm-air temperature perturbation extends up to 700 hPa during winter, summer, and fall, while the cold-air temperature perturbation extends to about 850 hPa for these seasons. One notable deviation from this pattern occurs during the LST^{-10} simulation during spring when 2-m air temperatures over three upper Great Lakes is warmer than the LST^{0} simulation. We hypothesis that this is due to an extended period of seasonal ice into the spring months. During

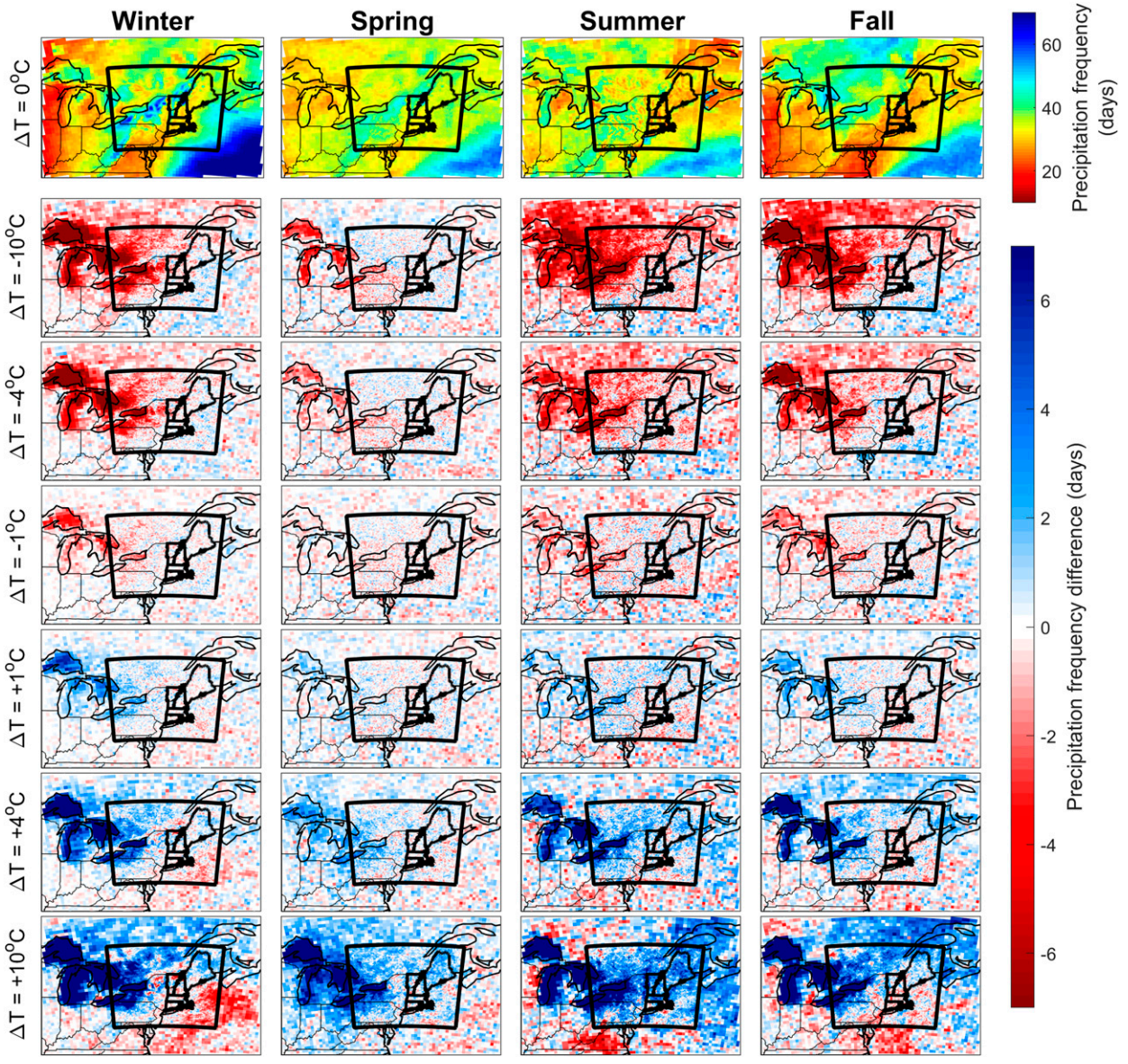

FIG. 10. As in Fig. 8, but for precipitation frequency (average number of wet days).

March–April, Lakes Superior, Michigan, and Huron are virtually 100% frozen, and only Lake Michigan drops below 75% ice cover during May (see monthly ice cover values in Table S4 of the online supplemental material). As nearby land surfaces begin to warm this time of year, the presence of ice cover reduces the localized cooling that would normally occur as ice retreats and the water surface is exposed to the overlying atmosphere. Only the air temperature over Lake Erie is colder in this simulation during spring, likely resulting from it being the first to become ice free during the warm season (only 22% remained ice covered in May) due to LSTs that warm above freezing by April (Fig. 4).

An examination of other atmospheric variables (Fig. 12), including sea level pressures, 700-hPa mixing ratios, and 500-hPa heights, illustrates how differences in moisture and temperature transport from the lakes modify synoptic-scale features. Higher LSTs produced lower sea level pressures and higher upper-level heights over most of the northeastern United States and southeastern Canada. This pattern is indicative of higher atmospheric thicknesses coinciding with warmer air temperatures in agreement with the hypsometric relationship. There are two notable exceptions. One is during spring for LST^{-10}, when no pressure anomalies are present, which agrees with the behavior of the overlake air temperatures as discussed in the previous paragraph. The other is during summer for LST^{+10} when 500-hPa heights are near the baseline values for the northern region and slightly below for the southern region. Atmospheric moisture at 700 hPa is higher for LST^{+10} during all seasons, with the strongest signal during summer and fall. There is a notable decrease in atmospheric moisture for

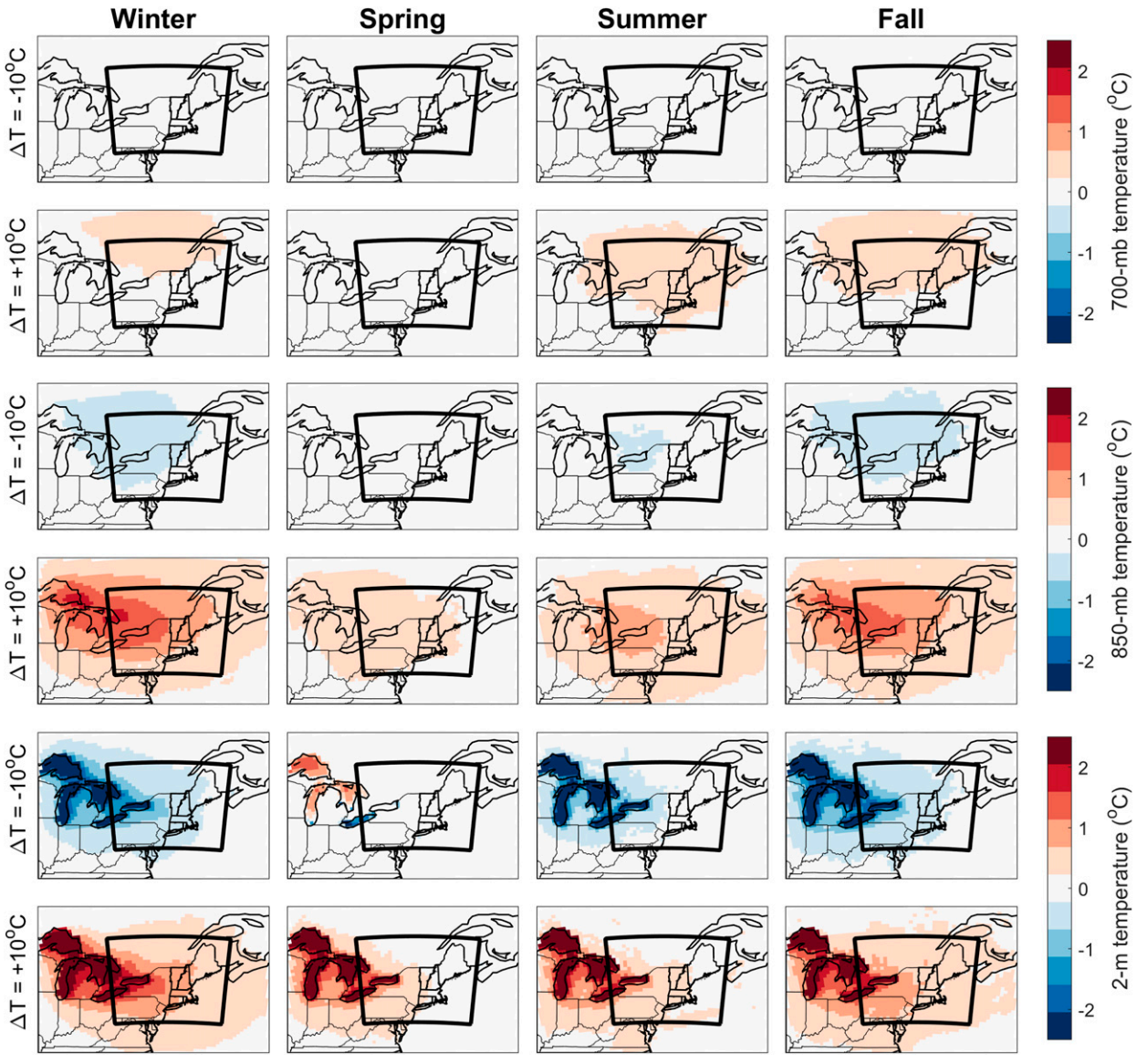

FIG. 11. Difference in seasonal average temperature between $\Delta T = \pm 10$°C simulations and $\Delta T = 0$°C simulation at various vertical levels. Only means that were significantly different from the baseline simulation according to a two-sided t test ($p < 0.05$) are shown.

LST^{-10} during summer and fall, but no statistical difference from baseline values during winter and spring.

4. Discussion

By quantifying how simulated precipitation and other atmospheric variables are altered when an RCM is run with warmer and colder LSTs, we can determine how much error may be introduced when erroneous LSTs are used as lower boundary conditions. We find that Great Lakes surface temperature perturbations are statistically correlated with simulated precipitation in New England but that the change in magnitude of spatially averaged values in this region is relatively small. The impact is largest during the summer, when precipitation increases by 7% over the LST^{-10} to LST^{+10} span. When considering spatial variability within New England, however, the annual difference in precipitation approaches 10% in some regions, with wetter conditions throughout Maine and drier conditions in other isolated regions, with increasing LSTs.

The impacts of LST changes on simulated precipitation are considerably larger to the north and south of central New England, which falls on a wet–dry line of a larger bimodal distribution. Wetter and drier regions emerged to the north for LST^{+10} and LST^{-10}, respectively, with precipitation differences in excess of 40% in some areas as far as 1000 km from the Great Lakes. This pattern arose in all seasons but is strongest during summer and fall. Differences in seasonal

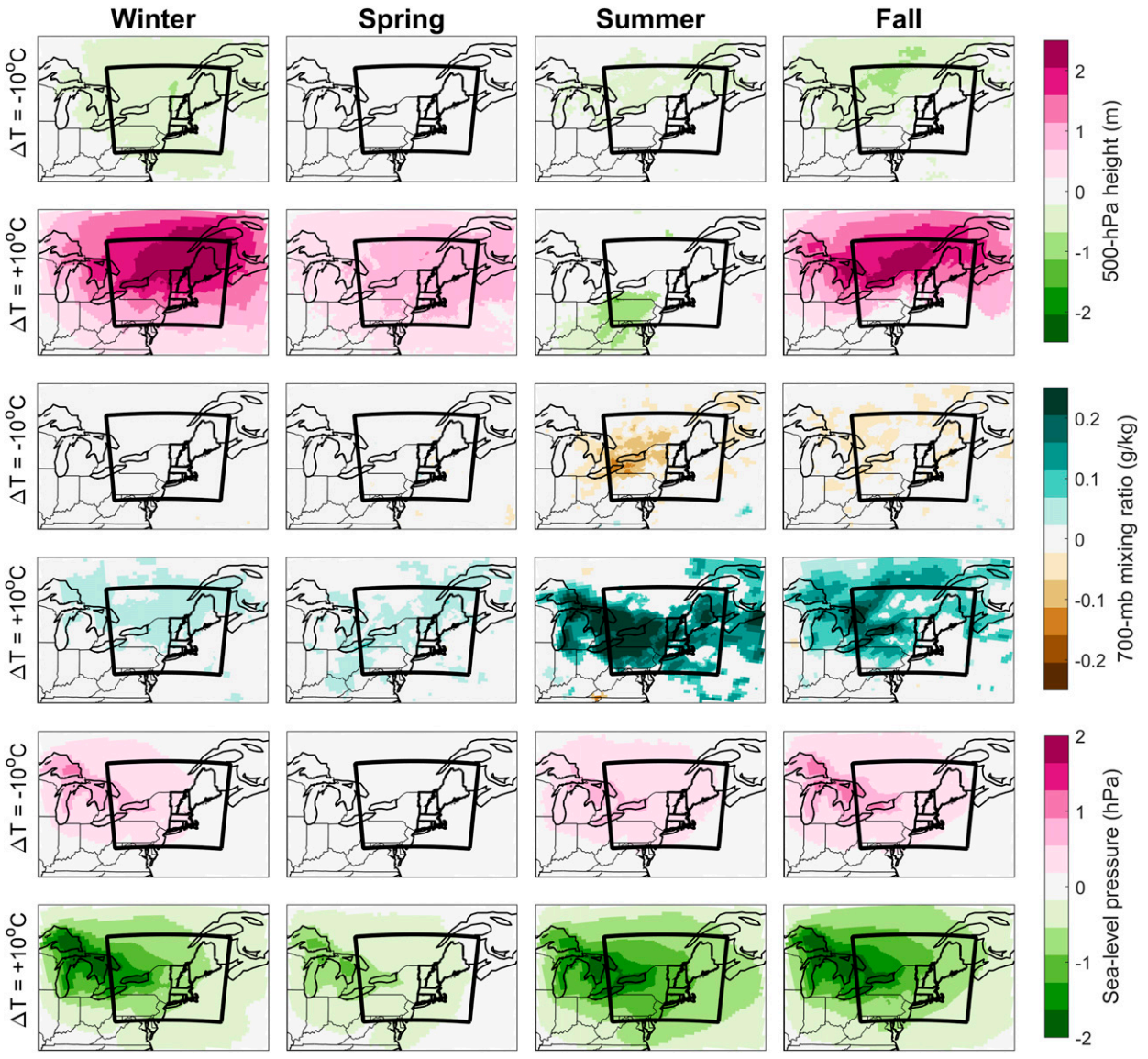

FIG. 12. As in Fig. 11 but for other atmospheric variables.

precipitation totals are largely attributed changes in the number of wet days in the northeastern United States and southeastern Canada. This is somewhat modified by changes in average intensity during the warm season, when more intense precipitation was simulated over the lakes and southeastern Canada, but less intense over the New England region, for LST^{+10}.

We find that the occurrence of more frequent wet days in the northeastern United States and southeastern Canada during LST^{+10} simulations is in part driven by the presence of thermally induced anomalous near-surface low pressure centered over the Great Lakes. This region is coincident with higher 500-hPa heights (with one exception of near-baseline heights during the summer), indicating higher atmospheric thicknesses resulting from warmer air temperatures throughout the lower atmosphere. In correspondence with the circulation of the anomalous low, atmospheric moisture is enhanced over much of the region for LST^{+10}, particularly during the warm season. While some of this additional moisture is likely a direct consequence of warmer water evaporating more moisture into the overlying atmosphere, which is advected downwind, the anomalous low pressure in the region also serves to transport moisture from the North Atlantic as indicated by the southerly near-surface geostrophic flow along the New England coastline.

These results are generally in agreement with Spero et al. (2016), who compared regional climate variables simulated by WRF when a lake model was used to estimate LSTs with simulations using WRF's nearest-neighbor preprocessing approach. They identified differences in LSTs between the simulations of up to 14° and 23°C during July and December, respectively, with the lake model on the cold side. Such

differences, however, were highly variable from one lake to the next and even within single lakes. Our LST^{-10} results are therefore similar in experimental design, with the exception that our temperature perturbations were spatially uniform. In lake regions where the temperature differential was of the same sign and comparable magnitude, we find commonalities. For example, Spero et al. (2016) identified higher sea level pressure over, and slightly downwind of, colder lake surfaces during summer and winter (their Figs. 6 and 7, respectively), similar in magnitude to pressure anomalies identified here (Fig. 12). They also determined that fewer wet days occurred in the vicinity of colder LSTs during the cold season (their Fig. 8), in agreement with our findings of less frequent precipitation for LST^{-} simulations (Fig. 10). Of interest is that, although our outer model domain was of the same spatial resolution as Spero et al. (2016) and encompassed regions where they observed large-scale pressure and temperature oscillations (cf. our Fig. 1 with their Figs. 6–8), our LST perturbations did not produce such features. We hypothesize that this is due to the homogeneity of our temperature alterations, which is in contrast to one of their simulations that used WRF-assigned temperatures that were incongruous across lake surfaces.

5. Summary

Great Lakes surface temperatures are often not provided by driving GCMs and must therefore be estimated for inclusion with lower boundary conditions as required by RCMs. The temperatures can be estimated a number of ways, some of which have the potential to introduce large errors (Gao et al. 2012; Bullock et al. 2014; Mallard et al. 2015; Spero et al. 2016). In addition, given that large inland water bodies have been warming disproportionate to land (Schneider and Hook 2010; O'Reilly et al. 2015; Zhong et al. 2016)—a trend that is expected to continue (Austin and Colman 2007), real-world LST values may not be accurately captured in future climate simulations.

By running an RCM with substantially warmer and colder Great Lakes surface temperatures, we investigated how erroneous values can impact simulated precipitation in New England and the surrounding region. We used WRF to downscale ERA-Interim reanalysis data using a one-way, two-domain model configuration centered over the northeastern portion of the United States, with the Great Lakes fully encompassed by the outer domain. Lake surface temperatures from the ERA5 reanalysis dataset were used for a baseline simulation. These temperatures were then perturbed by up to ±10°C over a 5-yr period and used as lower-boundary conditions for additional simulations.

As LSTs are warmed above the baseline scenario, the WRF simulation produces higher evaporative losses from the Great Lakes and virtually eliminates ice cover year-round. As LSTs are cooled, evaporative losses systematically decrease throughout the year and ice cover extent increases. We find that simulated precipitation in New England is statistically correlated with LST perturbations, but this region falls on a wet–dry line of a larger bimodal distribution, with wetter conditions to the north and drier conditions to the south with increasing LSTs. Relatively small LST perturbations (up to ±2°C) only minimally impact spatially averaged precipitation, but the influence of LSTs becomes larger with increasing magnitude of perturbations, particularly during the warm season. To the north of New England, simulated total precipitation differs by up to 40% as far as 1000 km from the Great Lakes with larger LST perturbations. This difference in precipitation is largely driven by changes in the number of wet days. Warmer lake surfaces produce anomalously low surface pressure and high upper-level heights over much of the region. Near-surface southerly geostrophic flow is enhanced along the East Coast with warm LSTs, particularly during the summer, thus transporting Atlantic moisture inland and contributing to higher precipitation amounts during this season.

This analysis illustrates how erroneous Great Lakes surface temperatures might influence precipitation statistics generated by regional climate models, even in regions located far from the basin. The precipitation differences identified here coincide with large-scale anomalous temperature, pressure, and moisture patterns. Care must therefore be taken to ensure reasonably accurate Great Lakes surface temperatures when simulating precipitation, especially in southeastern Canada, Maine, and the mid-Atlantic region.

This work of understanding the sensitivity of WRF to varying LSTs could be enhanced in a few ways. First, because only one model configuration was used here, other commonly employed setups should be examined. Some suggested alterations include the use of higher-resolution domains and relocating or resizing of the domains over the lakes and surrounding regions. Different model physics might also be used, such as boundary layer schemes and cumulus parameterizations. In particular, because the thermal diffusion scheme used here is a relatively simple land surface option (Jin et al. 2010), other WRF options could be explored. In addition, because large-scale oscillations in atmospheric pressure and moisture identified by Spero et al. (2016) were not observed in the present simulations, additional simulations with abrupt lake-to-lake temperature discontinuities are worthwhile to confirm that such phenomena are the result of spatially incongruous temperatures as opposed to drastic, but spatially uniform, temperature perturbations. Also, because our simulations incorporated identical temperature perturbations throughout the year, the enhanced warming of Great Lakes surface water during the summer months (Austin and Colman 2007) was not represented. An examination of this dynamic may be worthwhile to better understand how seasonally dependent warming might modify model results.

Acknowledgments. This work was supported by the National Science Foundation through VT EPSCoR (Award OIA-1556770). We acknowledge high-performance computing support from Cheyenne (https://doi.org/10.5065/D6RX99HX) provided by NCAR's Computational and Information Systems Laboratory, sponsored by the National Science Foundation. Author Huang acknowledges support from the U.S. Department of Energy Office of Science, Office of Biological and Environmental Research, Climate and Environmental Sciences Division, Regional and Global Model Analysis Program, under Award

DE-AC02-05CH11231. Figures 11 and 12 were created using the colorbrewer schemes for Matlab (https://www.mathworks.com/matlabcentral/fileexchange/34087-cbrewer-colorbrewer-schemes-for-matlab), MATLAB Central File Exchange. We thank Drs. David Siuta and George Loriot for productive conversations and helpful feedback, Jason Kaiser for his technical assistance, and three anonymous reviewers for their constructive feedback.

REFERENCES

Anyah, R., and F. Semazzi, 2004: Simulation of the sensitivity of Lake Victoria basin climate to lake surface temperatures. *Theor. Appl. Climatol.*, **79**, 55–69, https://doi.org/10.1007/s00704-004-0057-4.

Austin, J., and S. Colman, 2007: Lake Superior summer water temperatures are increasing more rapidly than regional air temperatures: A positive ice-albedo feedback. *Geophys. Res. Lett.*, **34**, L06604, https://doi.org/10.1029/2006GL029021.

Bullock, O. R., K. Alapaty, J. A. Herwehe, M. S. Mallard, T. L. Otte, R. C. Gilliam, and C. G. Nolte, 2014: An observation-based investigation of nudging in WRF for downscaling surface climate information to 12-km grid spacing. *J. Appl. Meteor. Climatol.*, **53**, 20–33, https://doi.org/10.1175/JAMC-D-13-030.1.

Burakowski, E. A., S. V. Ollinger, G. B. Bonan, C. P. Wake, J. E. Dibb, and D. Y. Hollinger, 2016: Evaluating the climate effects of reforestation in New England using a Weather Research and Forecasting (WRF) Model multiphysics ensemble. *J. Climate*, **29**, 5141–5156, https://doi.org/10.1175/JCLI-D-15-0286.1.

Copernicus Climate Change Service, 2017: ERA5: Fifth generation of ECMWF atmospheric reanalyses of the global climate. Copernicus Climate Change Service Climate Data Store, accessed 7 July 2019, https://cds.climate.copernicus.eu/cdsapp#!/home.

Dee, D. P., and Coauthors, 2011: The ERA-Interim reanalysis: Configuration and performance of the data assimilation system. *Quart. J. Roy. Meteor. Soc.*, **137**, 553–597, https://doi.org/10.1002/qj.828.

Easterling, D. R., and Coauthors, 2017: Precipitation change in the United States. *Climate Science Special Report: Fourth National Climate Assessment*, D. J. Wuebbles et al., Eds., Vol. I, U.S. Global Change Research Program, 207–230.

Frich, P., L. Alexander, P. Della-Marta, B. Gleason, M. Haylock, A. Klein Tank, and T. Peterson, 2002: Observed coherent changes in climatic extremes during the second half of the twentieth century. *Climate Res.*, **19**, 193–212, https://doi.org/10.3354/cr019193.

Gao, Y., J.S. Fu, J.B. Drake, Y. Liu, and J.F. Lamarque, 2012: Projected changes of extreme weather events in the eastern United States based on a high resolution climate modeling system. *Environ. Res. Lett.*, **7**, 044025, https://doi.org/10.1088/1748-9326/7/4/044025.

Guilbert, J., A. Betts, D. Rizzo, B. Beckage, and A. Bomblies, 2015: Characterization of increased persistence and intensity of precipitation in the northeastern United States. *Geophys. Res. Lett.*, **42**, 1888–1893, https://doi.org/10.1002/2015GL063124.

Gula, J., and W. Peltier, 2012: Dynamical downscaling over the Great Lakes Basin of North America using the WRF regional climate model: The impact of the Great Lakes system on regional greenhouse warming. *J. Climate*, **25**, 7723–7742, https://doi.org/10.1175/JCLI-D-11-00388.1.

Hanrahan, J., S. Kravtsov, and P. Roebber, 2010: Connecting past and present climate variability to the water levels of Lakes Michigan and Huron. *Geophys. Res. Lett.*, **37**, L01701, https://doi.org/10.1029/2009GL041707.

——, A. Maynard, S. Murphy, C. Zercher, and A. Fitzpatrick, 2017: Examining the climatology of shortwave radiation in the northeastern United States. *J. Appl. Meteor. Climatol.*, **56**, 2869–2881, https://doi.org/10.1175/JAMC-D-16-0420.1.

Hayhoe, K., J. VanDorn, T. Croley, N. Schlegal, and D. Wuebbles, 2010: Regional climate change projections for Chicago and the US Great Lakes. *J. Great Lakes Res.*, **36**, 7–21, https://doi.org/10.1016/j.jglr.2010.03.012.

Hoerling, M., J. Eischeid, J. Perlwitz, X. Quan, K. Wolter, and L. Cheng, 2016: Characterizing recent trends in U.S. heavy precipitation. *J. Climate*, **29**, 2313–2332, https://doi.org/10.1175/JCLI-D-15-0441.1.

Hong, S.-Y., and J.-O. Lim, 2006: The WRF single-moment 6-class microphysics scheme (WSM6). *J. Korean Meteor. Soc.*, **42**, 129–151.

Huang, H., J. Winter, E. Osterberg, R. Horton, and B. Beckage, 2017: Total and extreme precipitation changes over the northeastern United States. *J. Hydrometeor.*, **18**, 1783–1798, https://doi.org/10.1175/JHM-D-16-0195.1.

——, ——, ——, J. Hanrahan, C. Bruyère, P. Clemins, and B. Beckage, 2020: Simulating precipitation and temperature in the Lake Champlain basin using a regional climate model: Limitations and uncertainties. *Climate Dyn.*, **54**, 69–84, https://doi.org/10.1007/s00382-019-04987-8.

Hunter, T., A. Clites, K. Campbell, and A. Gronewold, 2015: Development and application of a North American Great Lakes hydrometeorological database—Part I: Precipitation, evaporation, runoff, and air temperature. *J. Great Lakes Res.*, **41**, 65–77, https://doi.org/10.1016/j.jglr.2014.12.006.

Iacono, M. J., J. S. Delamere, E. J. Mlawer, M. W. Shephard, S. A. Clough, and W. D. Collins, 2008: Radiative forcing by long-lived greenhouse gases: Calculations with the AER radiative transfer models. *J. Geophys. Res.*, **113**, D13103, https://doi.org/10.1029/2008JD009944.

Jiménez, P. A., J. Dudhia, J. F. González-Rouco, J. Navarro, J. P. Montávez, and E. García-Bustamante, 2012: A revised scheme for the WRF surface layer formulation. *Mon. Wea. Rev.*, **140**, 898–918, https://doi.org/10.1175/MWR-D-11-00056.1.

Jin, J., N. L. Miller, and N. Schlegel, 2010: Sensitivity study of four land surface schemes in the WRF model. *Adv. Meteor.*, **2010**, 167436, https://doi.org/10.1155/2010/167436.

Komurcu, M., K. A. Emanuel, M. Huber, and R. P. Acosta, 2018: High-resolution climate projections for the northeastern United States using dynamical downscaling at convection-permitting scales. *Earth Space Sci.*, **5**, 801–826, https://doi.org/10.1029/2018EA000426.

Mallard, M., C. Nolte, T. Spero, O. Bullock, K. Alapaty, J. Herwehe, J. Gula, and J. Bowden, 2015: Technical challenges and solutions in representing lakes when using WRF in downscaling applications. *Geosci. Model Dev.*, **8**, 1085–1096, https://doi.org/10.5194/gmd-8-1085-2015.

Notaro, M., K. Holman, A. Zarrin, E. Fluck, S. Vavrus, and V. Bennington, 2013: Influence of the Laurentian Great Lakes on regional climate. *J. Climate*, **26**, 789–804, https://doi.org/10.1175/JCLI-D-12-00140.1.

O'Reilly, C. M., and Coauthors, 2015: Rapid and highly variable warming of lake surface waters around the globe. *Geophys. Res. Lett.*, **42**, 10 773–10 781, https://doi.org/10.1002/2015GL066235.

Schneider, P., and S. Hook, 2010: Space observations of inland water bodies show rapid surface warming since 1985. *Geophys. Res. Lett.*, **37**, L22405, https://doi.org/10.1029/2010GL045059.

Scott, R., and F. Huff, 1996: Impacts of the Great Lakes on regional climate conditions. *J. Great Lakes Res.*, **22**, 845–863, https://doi.org/10.1016/S0380-1330(96)71006-7.

Skamarock, W. C., Coauthors, 2019: A description of the Advanced Research WRF Model version 4. NCAR Tech. Note NCAR/TN-556+STR, 145 pp., https://doi.org/10.5065/1dfh-6p97.

Spero, T., C. Nolte, J. Bowden, M. Mallard, and J. Herwehe, 2016: The impact of incongruous lake temperatures on regional climate extremes downscaled from the CMIP5 archive using the WRF Model. *J. Climate*, **29**, 839–853, https://doi.org/10.1175/JCLI-D-15-0233.1.

Trail, M., A.P. Tsimpidi, P. Liu, K. Tsigaridis, Y. Hu, A. Nenes, and A.G. Russell, 2013: Downscaling a global climate model to simulate climate change over the US and the implication on regional and urban air quality. *Geosci. Model Dev.*, **6**, 1429–1445, https://doi.org/10.5194/gmd-6-1429-2013.

Wang, J., X. Bai, H. Hu, A. Clites, M. Colton, and B. Lofgren, 2012: Temporal and spatial variability of Great Lakes ice cover, 1973–2010. *J. Climate*, **25**, 1318–1329, https://doi.org/10.1175/2011JCLI4066.1.

Wang, W., and Coauthors, 2017: User's guide for the Advanced Research WRF (ARW) Modeling System version 3.9. UCAR, 443 pp., https://www2.mmm.ucar.edu/wrf/users/docs/user_guide_V3/user_guide_V3.9/ARWUsersGuideV3.9.pdf.

Wright, D., D. Posselt, and A. Steiner, 2013: Sensitivity of lake-effect snowfall to lake ice cover and temperature in the Great Lakes region. *Mon. Wea. Rev.*, **141**, 670–689, https://doi.org/10.1175/MWR-D-12-00038.1.

Zhao, L., J. Jin, S. Wang, and M. Ek, 2012: Integration of remote-sensing data with WRF to improve lake-effect precipitation simulations over the Great Lakes region. *J. Geophys. Res.*, **117**, D09102, https://doi.org/10.1029/2011JD016979.

Zhong, Y., M. Notaro, S. Vavrus, and M. Foster, 2016: Recent accelerated warming of the Laurentian Great Lakes: Physical drivers. *Limnol. Oceanogr.*, **61**, 1762–1786, https://doi.org/10.1002/lno.10331.